Experimental study on tensile properties of 3D printed flexible kirigami specimens

Jun Nakajima[a], Kazem Fayazbakhsh[b,*], Yoshinori Teshima[a]

[a]*Department of Mechanical Science and Engineering, Chiba Institute of Technology, 2-17-1 Tsudanuma, Narashino, Chiba, 275-0016 Japan*
[b]*Aerospace Engineering Department, Ryerson University, 350 Victoria Street, Toronto, ON, Canada M5B 2K3*
**Corresponding author: kazem@ryerson.ca; Tel: (+1) 416-979-5000 ext. 6414; fax: (+1) 416-979-5056*

Abstract

Fused Filament Fabrication (FFF) is one of the most popular 3D printing processes that can be used to manufacture flexible parts. With the use of kirigami structures, the load-carrying capability and elongation of these parts can be significantly improved. In this work, we investigate the impact of stacking sequence, slit size, and thickness on the tensile properties of 3D printed flexible kirigami specimens. In addition, we demonstrate how the transition phenomenon and out-of-plane deformation can significantly improve percent elongation at their breaking point. Considering the deformed shape during testing, specimens with a combination of layers printed along and transverse to their length showed the highest tensile break strength and the percent break elongation (2.43 MPa and 183 %, respectively). It is also determined that the occurrence of the transition phenomenon depends on the specimen's thickness, and was observed for the 1 mm and 1.5 mm thick samples.

Keywords:
kirigami; flexible material; Fused Filament Fabrication (FFF); tensile break strength; percent break elongation.

Additive Manufacturing. March 2020, 101100
https://doi.org/10.1016/j.addma.2020.101100

1. Introduction

Fused Filament Fabrication (FFF) is one of the most common 3D printing techniques and can manufacture parts from a wide range of materials. In this field, the impact of the manufacturing process and design parameters on the tensile properties of FFF 3D printed parts made out of standard filament materials such as polylactic acid (PLA), acrylonitrile butadiene styrene (ABS), polycarbonate (PC), and polyamides are typically investigated. A summary of these results can be found in several review studies in which build orientation, raster angle, layer thickness, infill percentage, number of perimeters (shells), nozzle temperature, bed temperature, and printing speed are considered as variables [1-4]. It was concluded that specimens printed in the XZY build orientation (on-edge) generally yield superior tensile strength and modulus compared to XYZ (flat) followed by ZXY (up-right). In addition, a raster angle of 0° results in the highest ultimate tensile strength and elastic modulus. These values are reduced as the raster angle increases up to 90°. Layer thickness is a highly disputed parameter, and researchers have reported a variation in results. Some research studies have revealed a reduction in tensile strength and modulus, due to an increase of layer thickness [5-14], whereas others have reported a decrease followed by an increase in the tensile properties [15-16]. It should be noted that Ahn et al. [17] and Melenka et al. [18] did not identify a direct relationship between the layer height and the mechanical properties of FFF 3D printed parts. Investigators have concluded that an increase in the infill percentage significantly improves both the elastic modulus and the tensile strength of these printed components [1-4]. In addition, it was determined that increasing the number of perimeters leads to a higher tensile strength [2]. The nozzle, bed, and environment (or chamber) temperatures play a significant role in dimensional accuracy, surface quality, and the tensile properties of FFF 3D printed parts [2-3]. Printing speed/feed rate is associated with the manufacturing time and cost, and researchers have concluded that lower values result in higher tensile properties.

The aforementioned works explored standard filament materials and investigated several parameters to obtain desirable tensile properties, e.g., maximum tensile strength, modulus, or strain at break. For certain applications, e.g., wearable and assistive devices, the use of flexible materials is essential because target failure strains cannot be achieved only by the appropriate selection of design and manufacturing process parameters for standard materials. Although there have been extensive studies on tensile testing of FFF 3D printed parts made from standard filament materials [1-4], there is limited published data on printed components fabricated using flexible materials such as thermoplastic elastomer (TPE), thermoplastic polyurethane (TPU), and ethylene-vinyl acetate (EVA).

Kumar et al. [19] developed an in-house computer numerical control (CNC) material deposition tool (MDT) to process EVA in pellet form to overcome the limitations of the FFF process with respect to elastomer processing. They performed an experimental study and identified the optimum barrel temperature and screw speed for high-quality part fabrication. Using optimum process parameters, they produced several 3D printed parts with different geometries and complexity, including a tensile test specimen. In a subsequent study [20], they manufactured five test specimens per ASTM D412 C, and performed tensile, hysteresis, and hardness tests. In addition, they performed measurements to determine dimensional accuracy and used microscopic analysis to investigate bonding between rasters. The ultimate tensile

strength (UTS) and the percent break elongation were obtained, and the values were compared to the properties of ABS and PLA material obtained from the literature. The average UTS and percent break elongation were 9.63 MPa and 575.5 %, respectively. This corresponded to an increase of up to 550 % in percent break elongation compared to ABS and PLA materials. In a later study [21], they fabricated 27 tensile specimens in total using a desktop 3D printer, and investigated the effect of barrel temperature, bed temperature, build orientation, raster angle, and the number of shells on the UTS and percent break elongation. It was observed that the tensile properties increased significantly with an increase in the barrel temperature. The platform temperature had a marginal effect on the UTS, whereas its effect on the percent break elongation was noticeable. The results of the analysis of variance (ANOVA) revealed that the build orientation had a marginal impact on the tensile properties. The specimen with a raster angle of 0° attained the highest UTS, while this value was a minimum at 90°. With an increase in the number of contours, the percent break elongation decreased, whereas the UTS was observed to increase, followed by a small decrease. The highest values obtained for the UTS and percent break elongation were 8.83 MPa and 522.34 %, respectively. The aforementioned studies confirmed that EVA can be used to make flexible parts for various applications, e.g., wearables. However, they only focused on the material, and did not investigate the application of novel geometric structures to improve the tensile properties of 3D printed parts.

Geometric structures such as kirigami can be used to increase the elongation and durability of manufactured parts. In this investigation, kirigami is limited to geometric structures with regular position slits [22]. "Kiri" and "Gami" in the Japanese word “kirigami” means "cut" and "paper," respectively [23] (Figure 1).

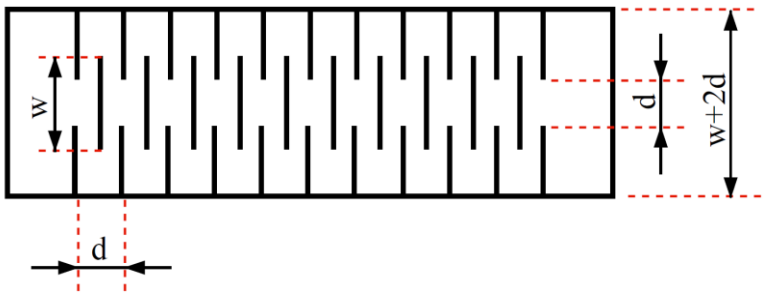

Figure 1. Simplified kirigami sheet.

Okumura et al. [22-23] used Kent paper as the material and derived equations for the relationship between the elastic constant, the cutting length, w, and the cutting interval, d. For an initial deformation region for which in-plane deformation is maintained, the elastic constant, k_1, can be calculated using the following formula:

$$\mathbf{k_1 \sim E\frac{d^3 t}{w^3}}, \quad (1)$$

where **E** is Young's modulus of the solid sheet material before incisions are made and **t** is its thickness.

Kirigami structures have high stretchability owing to the transition phenomenon. The softness of this structure emerges as a result of a transition from two-dimensional to three-dimensional

deformation [23]. Although kirigami structures are known for their high stretchability, there is insufficient quantitative data on the relationship between their geometrical dimensions and tensile properties.

In this investigation, the break strength and percent break elongation of flexible kirigami specimens are obtained via tensile testing. The specimens are 3D printed out of thermoplastic polyurethane (TPU) filament using a commercial desktop printer. In the following sections, the specimen geometry and stacking sequence convention are initially described. Then, the manufacturing process and design parameters for 3D printing are outlined, followed by the testing procedure. The impact of the stacking sequence, slit size, and thickness on the tensile properties of kirigami specimens are presented. Finally, a discussion of the break strength and percent break elongation of 3D printed flexible kirigami specimens is presented, followed by the main conclusions and recommendations for future research.

2. Specimen design and manufacturing

In this section, the geometrical dimensions of kirigami specimens are described and a convention for the stacking sequence is presented. The manufacturing process and design parameters for the 3D printing of specimens are then presented followed by the testing procedure.

2.1. Specimen geometry and stacking sequence

In this study, a kirigami structure is defined as a part in which slits are perpendicular to the part length and the loading direction (Figure 2).

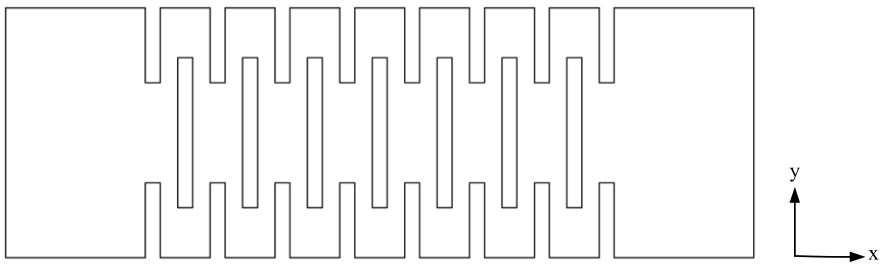

Figure 2. Kirigami specimen.

This structure is regarded as a serial connection of N kirigami unit-cells. Figure 3 shows a unit-cell in a kirigami specimen.

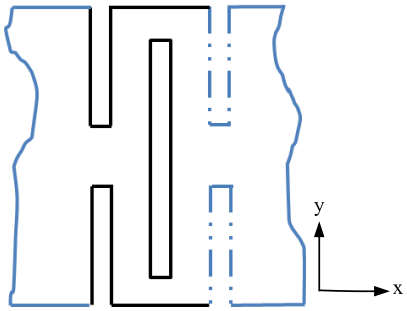

Figure 3. A unit-cell of a kirigami structure.

The number of kirigami unit-cells in the present experimental work is five, and the specimen geometry is shown in Figure 4. The kirigami unit-cell used in this investigation is characterized

by a Width (W) of each slit, vertical spacing (i) between the slits, horizontal spacing (d) between the slits, and the height (h) of each slit. Furthermore, there is a relationship between these dimensions in the kirigami as W > d and i >h. According to Figure 3 and 4, the kirigami unit-cell height is i+h and its width is W+d.

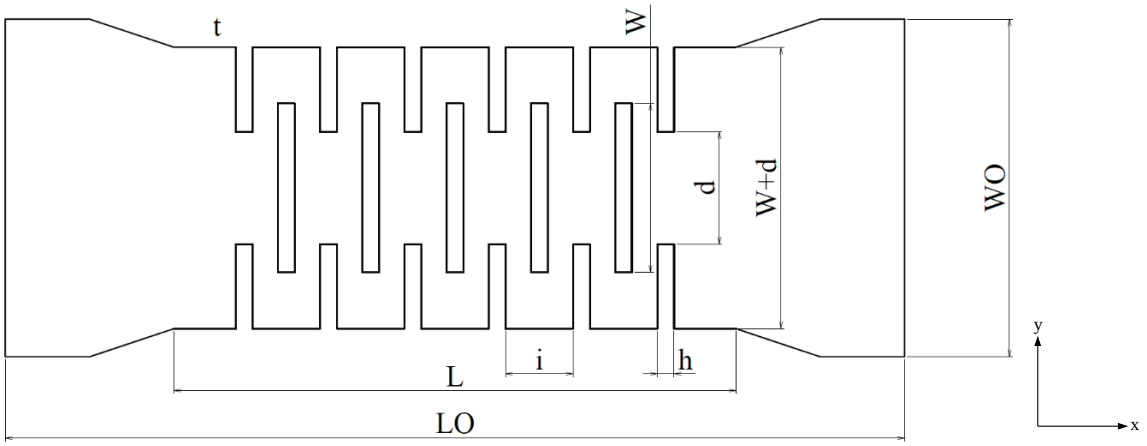

Figure 4. Geometry of Kirigami specimen.

Table 1 defines the dimensional parameters of kirigami specimens including gripping and overall dimensions.

Table 1. Dimensional parameters for the kirigami specimen.

Parameter	Description	Value (mm)
W	Slit Width	15
h	Slit Height	1
i	Slit interval	5
d	Distance between slit ends	10
t	Specimen thickness	2
W+d	Width of kirigami	25
L	Length between grips	50
LO	Overall length	80
WO	Width of the grip section	30

Slit height (h) of 1 mm is the minimum value for successful 3D printing without slits sticking together. Slit interval (i) is selected to satisfy the requirement of i > h in kirigami specimens in the study. There is no standardized test to follow for evaluating the tensile properties of flexible kirigami specimens made from thermoplastic polyurethane. However, ASTM D6693-04 (2015) [24] is recommended for determining tensile properties of non-reinforced polyethylene and nonreinforced flexible polypropylene. Its recommended gauge length for break of 50 mm is used for the length between grips (L) of kirigami specimens. The width of the grip section (WO = 30) is based on a custom-built fixture that will be used during testing (Section 2.2). Width of kirigami (W+d) of 25 mm is selected, which is less than WO, to create a gauge section and also dictates values for slit width (W) and distance between slit ends (d). W of 15 mm and d of 10 mm are selected to satisfy the requirement of W > d in kirigami specimens. Specimen thickness (t) of 2 mm is within the acceptable range per ASTM D6693-04, which is 0.25 mm to 6.3 mm.

Figure 5 illustrates the definition of the raster angle in which the loading direction is along the x-axis, the transverse of the loading direction is the y-axis, and the specimen thickness is along the z-axis.

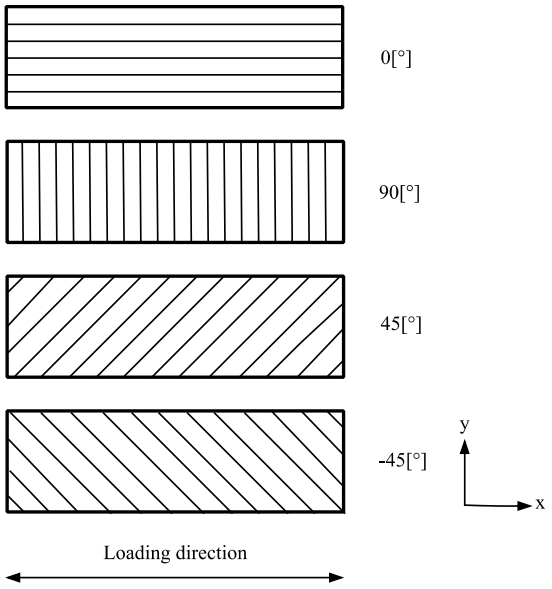

Figure 5. Raster angle definition.

Kirigami specimens have a stacking sequence that starts from the build plate. The printing pattern is a repetition of A1 and A2, where the first layer is A1 and the next layer is A2 (Figure 6).

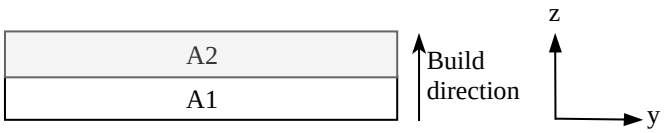

Figure 6. Definition of stacking sequence in kirigami specimens.

Per materials characterization approach used in composites, properties along (0° raster angles) and transverse (90° raster angles) to the extrudates are of interest. Furthermore, traditional layups, like cross-ply and angle-ply laminates are considered to provide reliable experimental data that can be used for validation of Finite Element (FE) models. Table 2 defines four different stacking sequences that were explored in this study, i.e. $[0/0]_n$, $[90/90]_n$, $[90/0]_n$, and $[45/-45]_n$.

Table 2. Specimen stacking sequences.

A1 orientation [°]	A2 orientation [°]	Stacking sequence
0	0	$[0/0]_n$
90	90	$[90/90]_n$
90	0	$[90/0]_n$
45	-45	$[45/-45]_n$

n: The number of repetitions for A1 and A2 pattern

2.2 Specimen manufacturing and testing procedure

Given that TPU is a soft material that presents challenges during 3D printing, manufacturing process parameters, especially the printing speed, were first optimized. One test specimen was manufactured using the default printing speed of 720 mm/min and subsequent specimens were printed while reducing the speed in increments of 10 % until high-quality parts were obtained. After manufacturing, the quality of the final specimens was examined via visual inspection. In total, eight specimens were 3D printed corresponding to printing speeds of 720 (default), 648, 576, 504, 432, 360, 288, and 216 mm/min. It was observed that at high printing speeds (720, 648, 504, and 432 mm/min), the hot end was not able to melt and extrude material through the nozzle at the required rates, resulting in a jammed nozzle and poor specimen quality. At the other end of the spectrum, for the lowest printing speed (216 mm/min), the material also did not extrude properly, due to dripping or the presence of bubbles in the layers. Considering the specimens printed at 360 mm/min and 288 mm/min that exhibited high quality, the latter was selected as the optimum printing speed because it resulted in a higher infill percentage. The manufacturing process and design parameters used for the 3D printing of the kirigami specimens are summarized in Table 3. A CR-10S desktop 3D printer (Creality 3D, Shenzhen, China) along with the Simplify3D software for slicing to control the printing parameters were used in this study. For all specimens, one shell was used on the perimeter of the specimens.

Table 3. Manufacturing and design parameters used for 3D printing.

Manufacturing/design Parameter	Value	Manufacturing/design Parameter	Value
Material	TPU	Bed temperature	70 °C
Build orientation	Z	Layer height	0.25 mm
Stacking sequence	$[90/90]_4$, $[0/0]_4$, $[90/0]_4$, $[45/-45]_4$	Printing speed	288 mm/min
Filament diameter	1.75 mm	Cooling	fan cooling
Nozzle diameter	0.4 mm	Infill	100%
Nozzle temperature	230 °C	# of shells	1

Five kirigami specimens were manufactured for each stacking sequence. Figure 7 shows the 3D printed kirigami specimens with a $[90/0]_4$ stacking sequence.

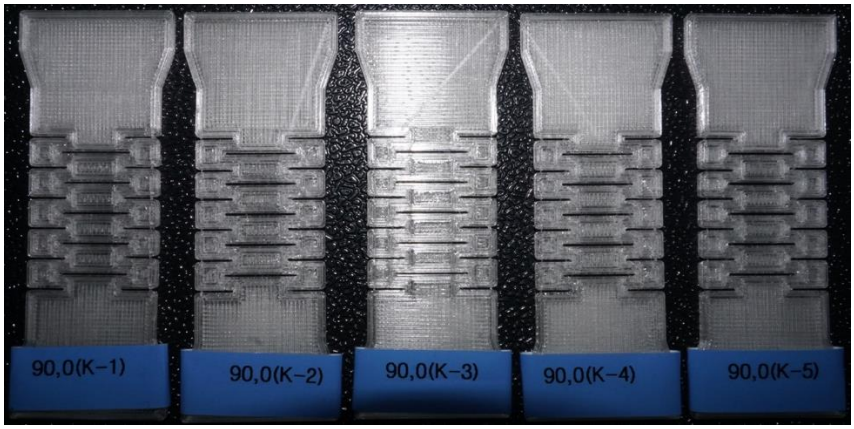

Figure 7. 3D printed kirigami specimens with $[90/0]_4$ stacking sequence.

For all specimens, the kirigami width and thickness were measured at three points (Figure 8), while every slit interval (i) and slit height (h) was measured at five points.

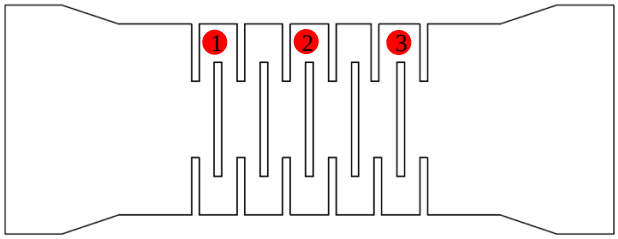

Figure 8. Measurement points for kirigami width and thickness.

Table 4 shows all measurements made for the 3D printed kirigami specimens with $[90/0]_4$ stacking sequence shown in Figure 7, along with their weights.

Table 4. Measurements for the 3D printed kirigami specimens with $[90/0]_4$ stacking sequence.

Specimen ID#	h (mm)	i (mm)	W+d (mm)	t (mm)	Weight (g)
90/0 K-1	0.96	4.91	24.8	2.24	5.10
90/0 K-2	1.02	4.96	24.7	2.32	5.10
90/0 K-3	1.05	4.93	24.9	2.32	5.01
90/0 K-4	1.10	5.05	25.0	2.25	4.95
90/0 K-5	1.09	5.11	25.0	2.29	5.10
Average	1.04	4.99	24.9	2.28	5.05
Standard deviation	0.057	0.085	0.125	0.038	0.069

All kirigami specimens were tested using a universal testing machine with a 2 kN load cell and the test speed was 50 mm/min (2 in/min). Figure 9 shows the test set-up including a kirigami specimen inside a custom-built fixture during testing. The grips were tightened evenly and firmly to prevent slippage of the specimens during the test.

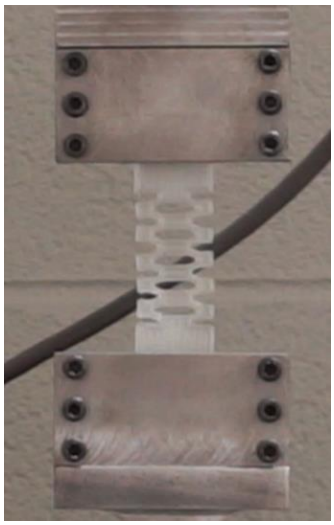

Figure 9. A kirigami specimen inside the fixture during a test.

3. Results and discussion

The load-extension curve for the specimens was recorded, and the load and extension at the break point were also obtained. The load was divided by the specimen width (W+d) and thickness (t), and was reported as the tensile break strength to three significant figures. The percent break elongation was calculated using the extension (change in the gauge length) at the break point divided by the gauge length (L = 50 mm), and was reported to the nearest 1 %.

3.1. The effect of specimen stacking sequence

Figure 10 shows a stress-extension curve for the kirigami specimens with $[90/0]_4$ stacking sequence until rupture.

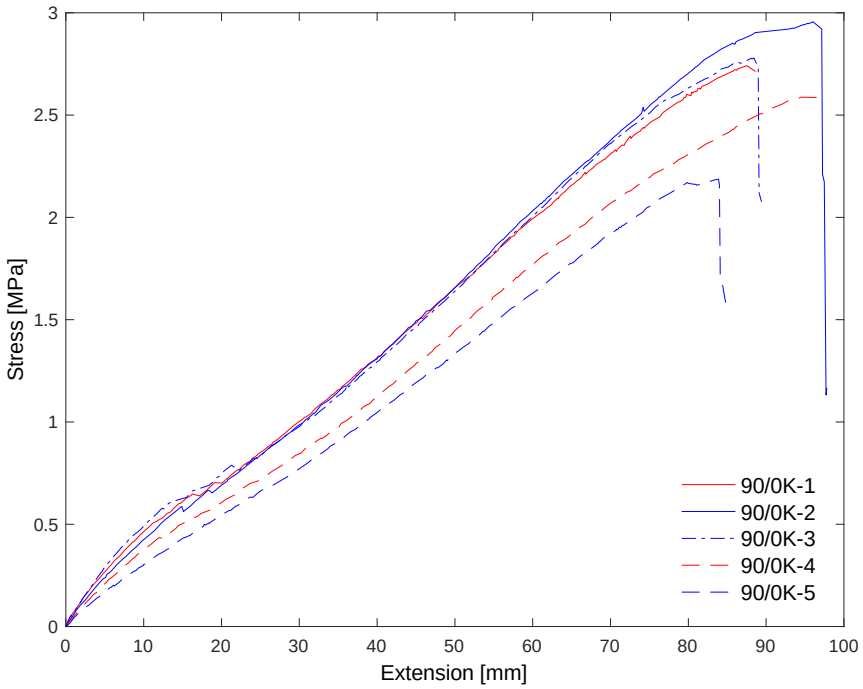

Figure 10. Stress-extension curve for the $[90/0]_4$ kirigami specimens.

Figure 11 shows the kigirami specimens with $[90/0]_4$ stacking sequence after testing.

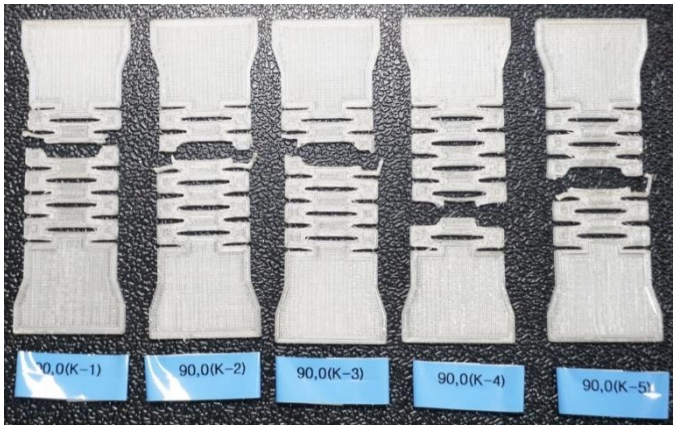

Figure 11. Fractured kirigami specimens with $[90/0]_4$ stacking sequence.

The test results for the kirigami specimens for all stacking sequences, i.e., $[90/90]_4$, $[0/0]_4$, $[90/0]_4$, $[45/-45]_4$ are summarized in Table 5, along with their Standard Deviation (SD) and Coefficient of Variation (CV).

Table 5. Tensile testing results for kirigami specimens with different stacking sequences.

Specimen	Average Tensile break strength [MPa]	SD [MPa]	CV %	Average percent break elongation [%]	SD [%]	CV %
$[0/0]_4$	2.16	0.248	11.5	158	9.93	6.30
$[90/90]_4$	1.81	0.409	22.6	184	49.1	26.7
$[45/-45]_4$	2.19	0.137	6.27	155	9.04	5.84
$[90/0]_4$	2.43	0.0419	1.73	183	8.55	4.66

It is evident that the kirigami specimens with the $[90/0]_4$ stacking sequence have the highest break strength (2.43 MPa), and their percent break elongation is very close to the maximum value (183 % for $[90/0]_4$ versus 184 % for the $[90/90]_4$ specimens). Kirigami specimens with $[90/90]_4$ have the lowest tensile break strength of 1.81 MPa; however, they have a maximum percent break elongation. All the kirigami specimens exhibited in-plane deformation and no sign of a transition to out of plane deformation (Figure 12). At the start of the test, the extrudates are along the loading direction for the $[0/0]_4$ specimens, and transverse to it for the $[90/90]_4$ specimens. As shown in Figure 12b, during testing, in the deformed specimens, both the $[0/0]_4$ and the $[90/90]_4$ samples exhibited regions where the extrudates are only transverse to the loading direction. In contrast, for the $[90/0]_4$ specimens, all regions have extrudates along the loading direction. Therefore, the $[90/0]_4$ specimens are expected to be more robust compared to the $[0/0]_4$ and $[90/90]_4$ specimens, and resisted the highest load, followed by the $[45/-45]_4$ specimens. This can be further confirmed by the very low CV of the $[90/0]_4$ specimens for both the tensile strength (1.7 %) and the percent break elongation (4.7 %), which were the minimum values among all specimens. In Figure 12, x_e is the extension in one Kirigami unit-cell during testing.

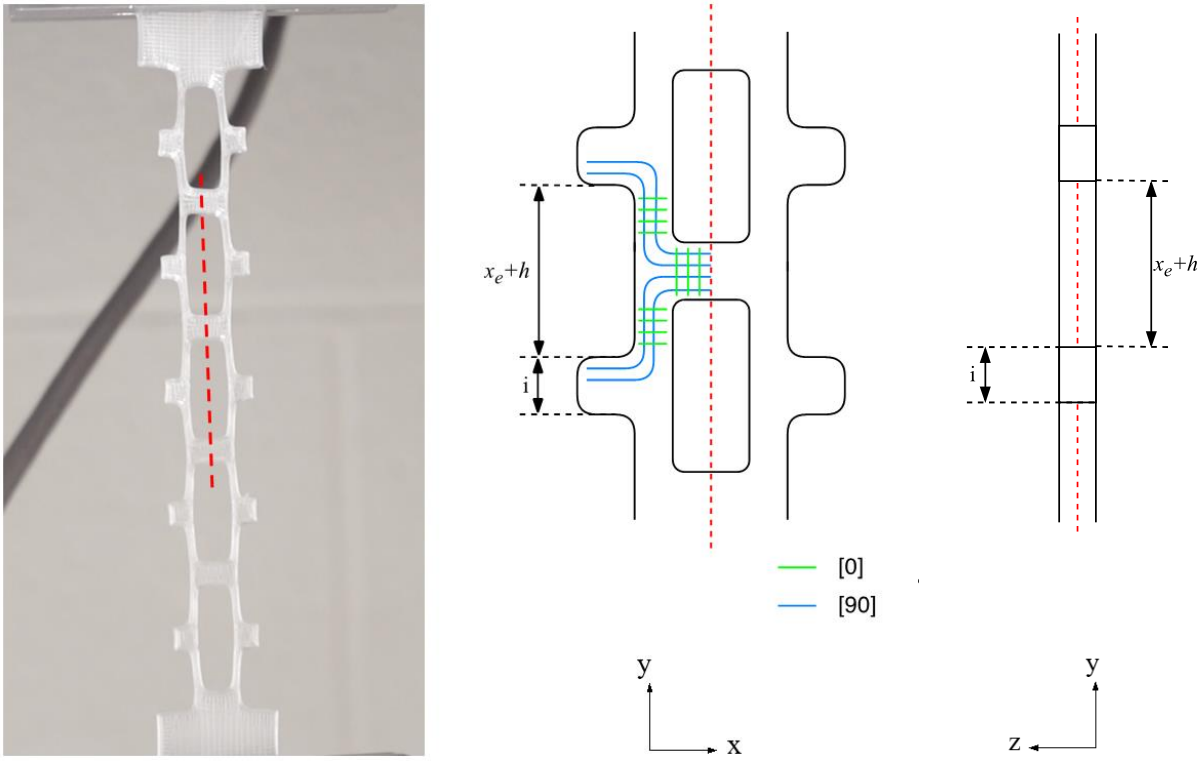

(a) **(b)** **(c)**

Figure 12. In-plane deformation of the kirigami specimens during testing: (a) Front view of a kirigami specimen; (b) front view of two kirigami unit cells showing the estimated extrudate paths in the deformed shape; and (c) side view of the kirigami showing only in-plane deformation.

The CV values for all specimens are small except for the $[90/90]_4$ samples, which have a CV of 22.6 % for the tensile break strength and 26.7 % for the percent break elongation. The CV obtained from the width and thickness measurements of the $[90/90]_4$ specimens are 0.5 % and 4.6 %, respectively. Therefore, the difference in the specimen geometry is not the reason for the high deviation of the tensile testing results. This can be explained by inspecting the nozzle path obtained from Simplify3D, the slicing software. As shown in Figure 13, there are gaps in the $[90/90]_4$ specimen transverse to the loading direction. During testing, cracks are initiated at these gaps and are propagated across the cross-section of the specimens, causing a large variation of the results.

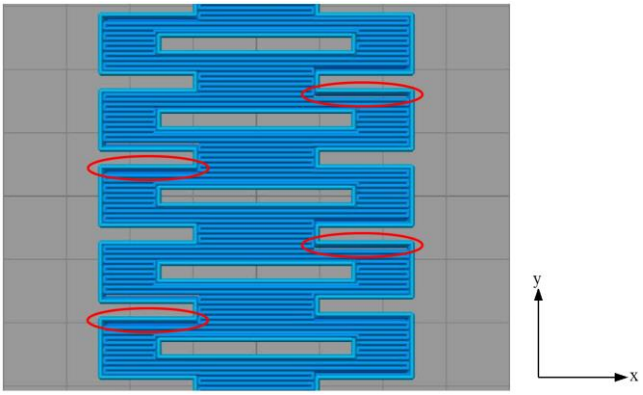

Figure 13. The nozzle path for a kirigami specimen with $[90/90]_4$ stacking sequence.

3.2. The effect of specimen slit size

Given that the $[45/-45]_4$ and $[90/0]_4$ stacking sequences have a high tensile break strength and are robust (low CV values), they were selected for further experimental testing to explore the impact of slit size. For these specimens, slit interval (i) was kept the same as the previous samples (5 mm), while the slit height (h) was increased from the initial minimum value of 1 mm to 2.5 mm in 0.5 mm increments (h = 1, 1.5, 2, and 2.5 mm). The slit height to interval ratio (h/i = 0.2, 0.3, 0.4, 0.5) was used to compare the tensile properties of the $[45/-45]_4$ and the $[90/0]_4$ kirigami specimens.

Five kirigami specimens were manufactured for each slit height using the manufacturing process and design parameters summarized in Table 3. Figure 14 shows kirigami specimens with a $[90/0]_4$ stacking sequence that was 3D printed with different slit heights.

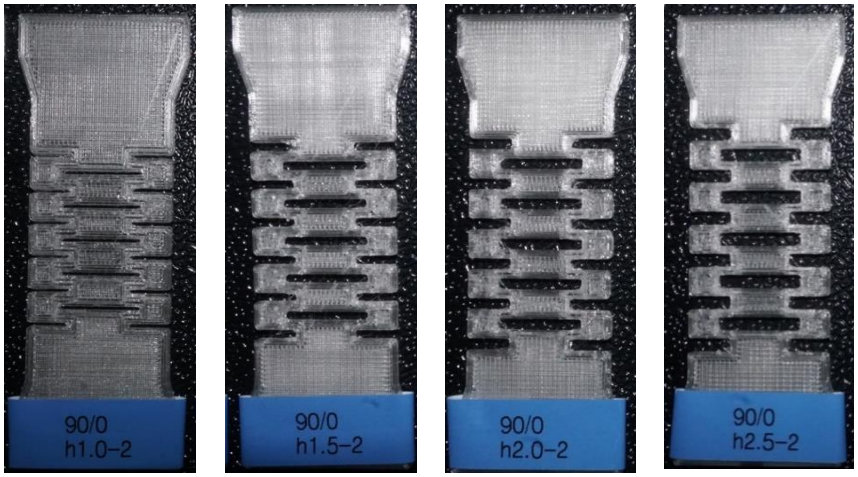

(a) (b) (c) (d)

Figure 14. Kirigami specimens with $[90/0]_4$ stacking and different slit heights, h: (a) 1 mm; (b) 1.5 mm; (c) 2 mm; and (d) 2.5 mm.

As explained in Section 2.2, for all specimens, the width and thickness were measured at three points (Figure 8), while every slit height (h) and slit interval (i) was measured at five points. Specimens were tested using the same load cell (2 kN) and the previously utilized test speed (50 mm/min). The load-extension curve was recorded, and the load and elongation at the break point were obtained. The tensile properties of the $[45/-45]_4$ and $[90/0]_4$ kirigami specimens as a function of slit height to interval ratio (h/i) are presented in Figure 15 and Figure 16, respectively. It should be noted that a higher slit height to interval ratio indicates a larger slit size.

As seen in Figure 15 and Figure 16, for both stacking sequences, $[45/-45]_4$ and $[90/0]_4$, an increase in the slit height to interval ratio from 0.2 to 0.5 does not necessarily imply a decrease in the tensile break strength. In addition, the relationship between the specimen tensile properties and h/i is different for the two stacking sequences. For the $[45/-45]_4$ specimens, with an increase in h/i, there is an initial increase in the tensile break strength and percent break elongation, followed by a sudden decrease in these properties that later improved. In contrast, for the $[90/0]_4$ specimens, there was a sudden reduction in the tensile properties, which were partially recovered with an increase in h/i. For the $[45/-45]_4$ specimens, a slit height to interval

ratio of approximately 0.321 has the highest tensile break strength and percent break elongation. For the $[90/0]_4$ specimens, h/i of 0.325 resulted in the minimum tensile properties, whereas the maximum values were achieved for h/i of 0.201.

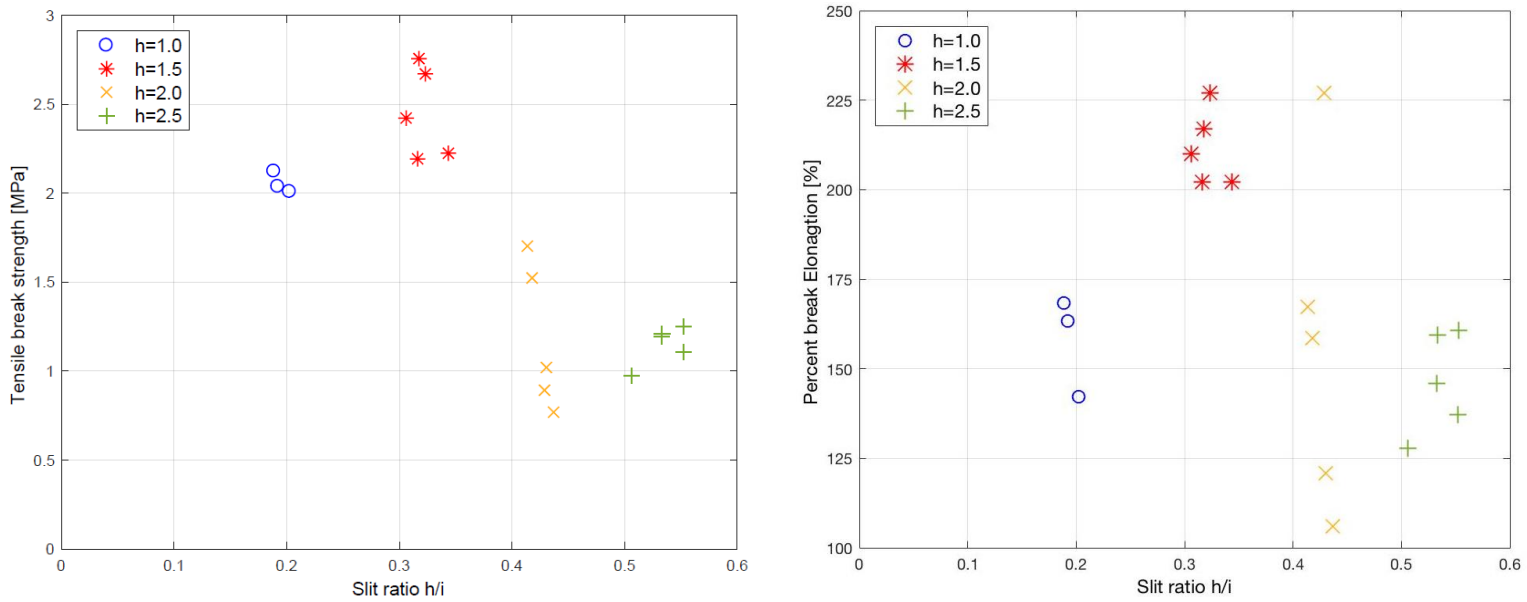

(a) **(b)**

Figure 15. Tensile properties of the $[45/-45]_4$ kirigami specimens for different slit height to interval ratio, h/i: (a) tensile break strength; and (b) percent break elongation.

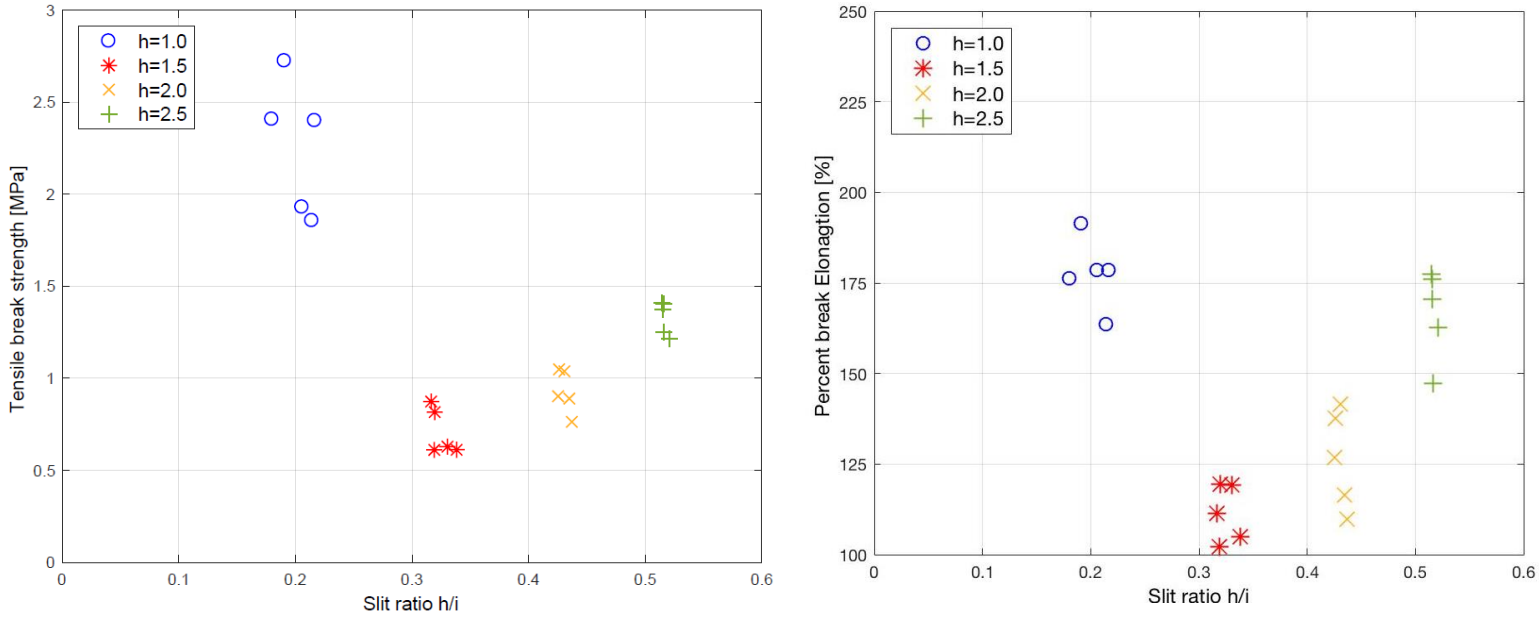

(a) **(b)**

Figure 16. Tensile properties of the $[90/0]_4$ kirigami specimens for different slit height to interval ratio, h/i: (a) tensile break strength; and (b) percent break elongation.

Using Eq. (1), the elastic constant was calculated and plotted against the slit height to interval ratio, h/i for the $[45/-45]_4$ and the $[90/0]_4$ specimens (Figure 17). The kirigami specimens with both stacking sequences have the highest elastic constant, k, for h/i of approximately 0.2. In contrast, the minimum k for the $[45/-45]_4$ specimens occurs at h/i of 0.5, whereas this value is 0.3 for the $[90/0]_4$ specimens. For the $[45/-45]_4$ specimens, the regression analysis revealed a quadratic fit with a higher coefficient of determination, R^2, compared to a linear fit (0.917 compared to 0.893). Both the linear and quadratic fits have a low R^2 for the $[90/0]_4$ specimens (0.386 and 0.825, respectively) compared to the $[45/-45]_4$ specimens.

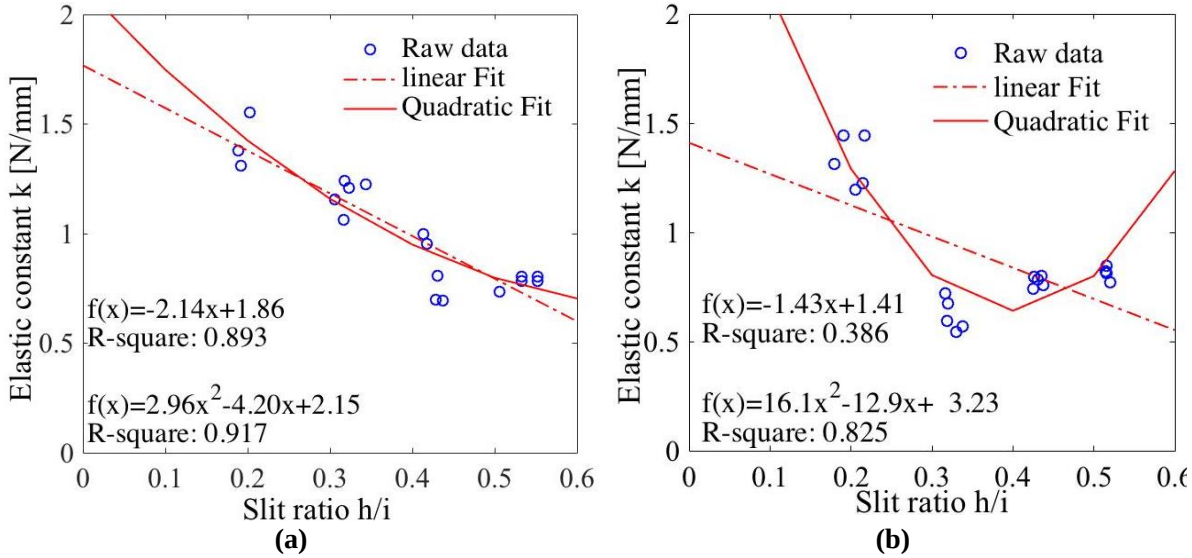

Figure 17. Elastic constant versus slit height to thickness ratio for kirigami specimens with different stacking sequences: (a) $[45/-45]_4$; and (b) $[90/0]_4$.

3.3. The effect of specimen thickness

In the cases investigated thus far, only in-plane deformation was observed, and the transition phenomenon did not occur. Given that the $[90/0]_4$ kirigami specimens have a high tensile break strength and are robust (Table 5), the $[90/0]_n$ stacking sequence was selected for further experimental testing to investigate the transition phenomenon. The original dimensions of the kirigami specimen (Table 1) were kept, and four thickness levels were investigated: 1 mm ($[90/0]_2$), 1.5 mm ($[90/0]_3$), 2 mm ($[90/0]_4$), and 2.5 mm ($[90/0]_5$). Five kirigami specimens were manufactured for each thickness level (stacking sequence) using the manufacturing process and design parameters shown in Table 3. Figure 18 shows one 3D printed kirigami specimen with the $[90/0]_n$ stacking sequence for each thickness level.

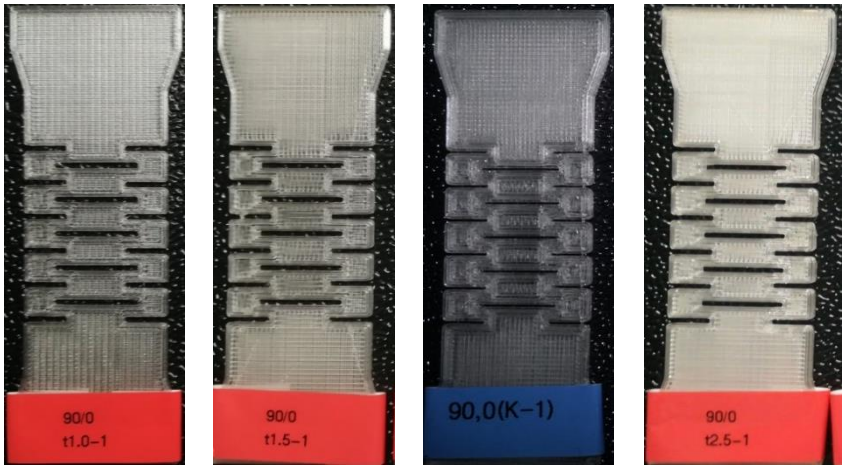

(a) **(b)** **(c)** **(d)**

Figure 18. Kirigami specimens with $[90/0]_n$ stacking for different thicknesses: (a) 1 mm; (b) 1.5 mm; (c) 2 mm; and (d) 2.5 mm.

As explained in Section 2.2, for all the specimens, the width and thickness were measured at three points, while every slit height (h) and slit interval (i) was measured. Specimens were tested using the same load cell (2 kN), and the test speed (50 mm/min) utilized for previous specimens. The load-extension curve was recorded, and the load, strength, and elongation at the break point versus specimen thickness are presented in Figure 19. According to Figure 19a, as expected, the tensile break load increases linearly with an increase in the specimen thickness (or cross-sectional area). The tensile break strength is almost constant and does not change with an increase in the specimen thickness (Figure 19b). Figure 19c shows that the percent break elongation also remains almost constant, because it is a material property and does not depend on the specimen thickness.

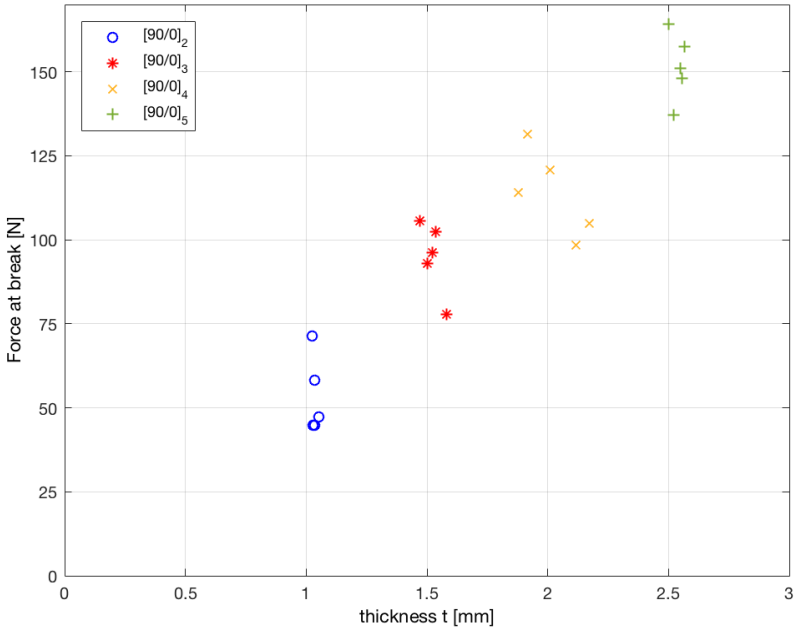
[90/0]2
[90/0]3
[90/0]4
[90/0]5
Force at break [N]
thickness t [mm]
0
25
50
75
100
125
150
0
0.5
1
1.5
2
2.5
3

(a)

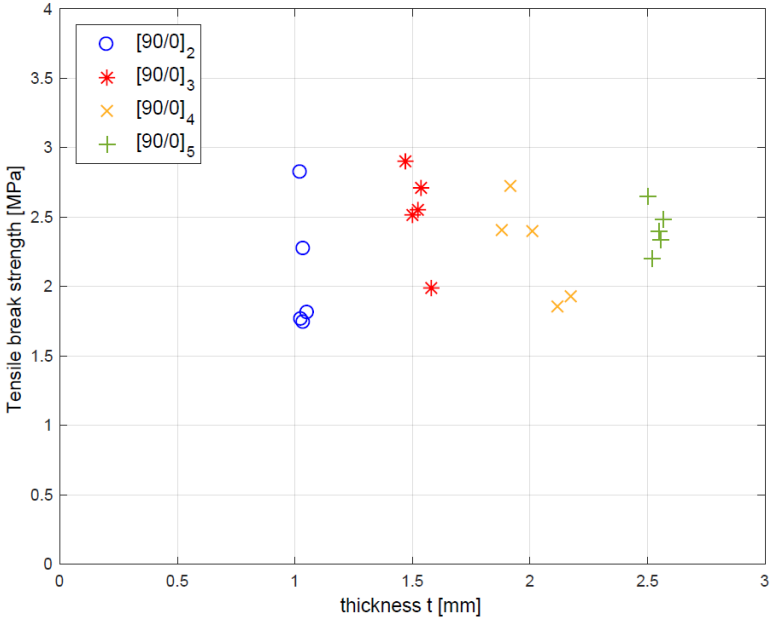
[90/0]2
[90/0]3
[90/0]4
[90/0]5
Tensile break strength [MPa]
thickness t [mm]
0
0.5
1
1.5
2
2.5
3
3.5
4
0
0.5
1
1.5
2
2.5
3

(b)

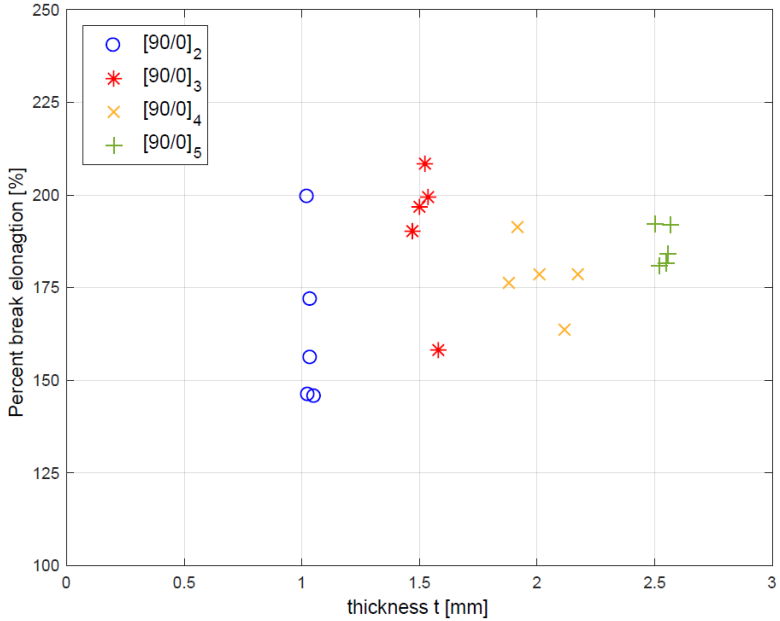

(c)

Figure 19. Tensile properties of the $[90/0]_n$ kirigami specimens with different thicknesses, t: (a) tensile break load; (b) tensile break strength; and (c) percent break elongation.

The large variation in percent break elongation for the specimens with 1 mm and 1.5 mm thickness compared to those with 2 mm and 2.5 mm thickness indicates that there is another influential phenomenon in the process of deformation until fracture. It is observed that the deformation of the specimens with 2 mm and 2.5 mm thickness is purely in-plane, whereas it is a combination of in-plane and out-of-plane (three-dimensional) for the 1 mm and 1.5 mm thick specimens. This can be clearly observed in Figure 20 for the kirigami specimen with a thickness of 1 mm. It can be concluded that the occurrence of the transition phenomenon depends on the specimen thickness. The test set-up used in this study facilitated the measurement of the machine cross-head movement and can only account for in-plane deformation. Future studies are required to characterize out-of-plane deformation for different kirigami configurations.

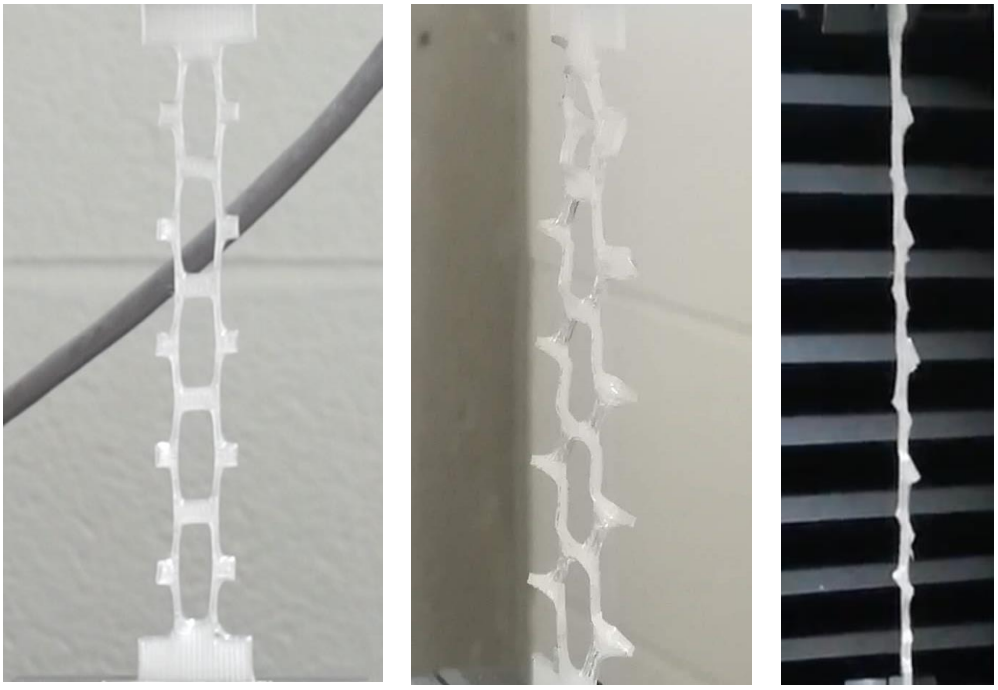

(a) **(b)** **(c)**

Figure 20. A $[90/0]_2$ kirigami specimen during testing showing three-dimensional deformation: (a) front; (b) isometric; and (c) side views.

4. Conclusions

The tensile properties of 3D printed flexible kirigami specimens were explored to investigate the impact of stacking sequence, slit size, and thickness. Kirigami specimens were designed and their geometrical dimensions were described along with a convention for the stacking sequence. They were manufactured out of thermoplastic polyurethane (TPU) using a commercial 3D printer. The stress-extension curve for the specimens was created, and the tensile break strength and extension at the break point were obtained. It was observed that the $[90/0]_4$ specimens have the highest tensile break strength and percent break elongation compared to the $[90/90]_4$, $[0/0]_4$, and the $[45/-45]_4$ specimens. For the $[90/0]_4$ and the $[45/-45]_4$ specimens, the slit height to interval ratio was varied. A ratio of 0.201 resulted in the maximum tensile properties for the $[90/0]_4$ specimens, whereas the ratio was 0.321 for the $[45/-45]_4$

specimens. In addition, it was observed that the occurrence of transition phenomenon depends on the specimen's thickness. The kirigami specimens with $[90/0]_2$ and $[90/0]_3$ stacking sequences (1 mm and 1.5 mm in thickness, respectively) exhibited a combination of in-plane and out-of-plane (three-dimensional) deformation compared to the pure in-plane deformation observed in the 2 mm and 2.5 mm thick specimens.

The optimum parameters for maximum load-carrying capability and elongation of the kirigami structures that were identified in this study can be used to design and print wearable devices for assistive devices. Wearable sleeve with actuators to improve the mobility of seniors is one potential application. In this study, the kirigami specimens consisted of five unit-cells, whereas a higher number connected in parallel and series is necessary for wearable devices. Future work is required to investigate the tensile properties of kirigami structures based on the results obtained in this study. The discrete homogenization method can be used to find equivalent properties of new kirigami structures and the acquired relationship between their tensile properties and geometric dimensions, based on the specimens investigated in this study.

Acknowledgment
This work is supported by the Natural Sciences and Engineering Research Council of Canada (NSERC), RGPIN-2018-04144, and a student exchange agreement between Chiba Institute of Technology and Ryerson University. We also would like to acknowledge Jordan Kalman for his consultation and technical support.

References

[1] Goh, G.D., et al., Process–Structure–Properties in Polymer Additive Manufacturing via Material Extrusion: A Review, Critical Reviews in Solid State and Materials Sciences, DOI: 10.1080/10408436.2018.1549977
[2] Rahim, T., et al., Recent Developments in Fused Deposition Modeling-Based 3D Printing of Polymers and Their Composites, Polymer Reviews, DOI: 10.1080/15583724.2019.15978833.
[3] Popescu, D., et al., FDM process parameters influence over the mechanical properties of polymer specimens: A review. Polymer Testing, 2018. 69: p. 157-166.
[4] Fayazbakhsh, K., M. Movahedi, and J. Kalman, The Impact of Defects on Tensile Properties of 3D Printed Parts Manufactured by Fused Filament Fabrication. Materials Today Communications, 2018.
[5] Li, H., Wang, T., Sun, J., Yu, Z., The effect of process parameters in fused deposition modelling on bonding degree and mechanical properties, Rapid Prototyp. J. 24 (1) (2018) 80–92 https://doi.org/10.1108/RPJ-06-2016-0090.
[6] Alafaghani, A. and Qattawi, A., Investigating the effect of fused deposition modeling processing parameters using Taguchi design of experiment method, J. Manuf. Process. 36 (2018) 164–174.
[7] Xiaoyong, S., Liangcheng, C., Honglin, M., Peng, G., Zhanwei, B., Cheng, L., Experimental analysis of high temperature PEEK materials on 3D printing test, 9th International Conference on Measuring Technology and Mechatronics Automation, 2017, pp. 13–16.
[8] Torres, J., Cole, M., Owji, A., DeMastry, Z., Gordon, AP., An approach for mechanical property optimization of fused deposition modeling with polylactic acid via design of experiments, Rapid Prototyp. J. 22 (2) (2016) 387–404.

[9] Ning, F., et al., Additive manufacturing of carbon fiber-reinforced plastic composites using fused deposition modeling: effects of process parameters on tensile properties, J. Compos. Mater. 51 (4) (2016) 451–462.
[10] Vidakis, N., et al., Fused deposition modelling parts tensile strength characterisation, Acad. J. Manuf. Eng. 14 (2) (2016).
[11] Salem, A., et al., 3-D printing and characterization of polymer composites with different reinforcements, Advanced Processing and Manufacturing Technologies for Nanostructured and Multifunctional Materials II: Ceramic Engineering and Science Proceedings Vol. 36 (6) (2015) 115–122.
[12] Tymrak, B.M., Kreiger, M., and Pearce, JM., Mechanical Properties of Components Fabricated with Open-Source 3-D Printers under Realistic Environmental Conditions. Materials & Design 58, 242-46 (2014).
[13] Onwubolu, Godfrey C., and Farzad Rayegani, Characterization and Optimization of Mechanical Properties of Abs Parts Manufactured by the Fused Deposition Modelling Process. International Journal of Manufacturing Engineering 2014, 13 (2014).
[14] Vaezi, M. and Chua, CK., Effects of Layer Thickness and Binder Saturation Level Parameters on 3d Printing Process. The International Journal of Advanced Manufacturing Technology 53, 275-84 (2011).
[15] Garg, A. and Bhattacharya A., An insight to the failure of FDM parts under tensile loading: finite element analysis and experimental study, Int. J. Mech. Sci. 120 (2017) 225–236.
[16] Sood, AK., Ohdar, RK., Mahapatra, SS., Parametric Appraisal of Fused Deposition Modelling Process Using the Grey Taguchi Method. Proceedings of the Institution of Mechanical Engineers, Part B: Journal of Engineering Manufacture 224, 135-45 (2010).
[17] Melenka, GW., Schofield, JS., Dawson, MR., Carey, JP., "Evaluation of dimensional accuracy and material properties of the makerbot 3D desktop printer", Rapid Prototyp. J. 2015, 21, 618–627. DOI: 10.1108/RPJ-09-2013-0093.
[18] Ahn, S., Montero, M., Odell, D., Roundy, S., Wright, PK., Anisotropic material properties of fused deposition modeling ABS", Rapid Prototyp. J. 2002, 8, 248–257. DOI: 10.1108/13552540210441166.
[19] Kumar, N., Jain, PK., Tandon, P., Pandey, PM. 3D printing of flexible parts using EVA material. Materials Physics and Mechanics 37 (2018) 124-132.
[20] Kumar, N., Jain, PK., Tandon, P., Pandey, PM. Extrusion-based additive manufacturing process for producing flexible parts. J Braz Soc Mech Sci Eng 2018;40:143. https://doi.org/10.1007/s40430-018-1068-x.
[21] Kumar, N., Jain, PK., Tandon, P., Pandey, PM. The effect of process parameters on tensile behavior of 3D printed flexible parts of ethylene vinyl acetate (EVA). Journal of Manufacturing Processes 35 (2018) 317–326.
[22] M. Isobe & K. Okumura, Initial rigid response and softening transition of highly stretchable kirigami sheet materials, Scientific Reports volume 6, Article number: 24758 (2016) https://www.nature.com/articles/srep24758.
[23] K. Okumura, M. Isobe and A. Takei, "Sheet material elasticity adjusting method, force sensor, and sheet material". Patent PCT/JP2017/015343, 14 April 2017.
[24] ASTM D6693. Standard Test Method for Determining Tensile Properties of Nonreinforced Polyethylene and Nonreinforced Flexible Polypropylene Geomembranes. ASTM International, West Conshohocken, PA, USA.